Progr. Theoret. Phys. (Kyoto) 37, 710 (1967); L. R. Ram Mohan, Phys. Rev. D1, 266 (1970).
[19]W. A. Simmons, Phys. Rev. 164, 1956 (1967); for a related application of this result, see D. S. Carlstone, S. P. Rosen and S. Pakvasa, Phys. Rev. 174, 1877 (1968), and L. R. Ram Mohan, Phys. Rev. D2, 2101 (1970).
[20]Y. T. Chiu, J. Schechter, and Y. Ueda, Phys. Rev. 157, 1317 (1967).
[21]Y. Hara and Y. Nambu, Phys. Rev. Letters 16, 875 (1966); D. K. Elias and J. C. Taylor, Nuovo Cimento 44A, 518 (1966); S. K. Bose and S. N. Biswas, Phys. Rev. Letters 16, 330 (1966); H. D. I. Abarbanel, Phys. Rev. 153, 1547 (1967).
[22]S. Weinberg, Phys. Rev. Letters 4, 87 (1960); 4, 585 (1960); G. Barton, C. Kacser, and S. P. Rosen, Phys. Rev. 130, 783 (1963).
[23]For a recent survey see B. H. Kellet, Nucl. Phys. B26, 237 (1971).
[24]N. Kroll and M. A. Ruderman, Phys. Rev. 93, 233 (1954).
[25]S. Okubo, Nuovo Cimento 41A, 586 (1966).

PHYSICAL REVIEW D VOLUME 4, NUMBER 2 15 JULY 1971

Duality and Single-Particle Production*

C. E. DeTar
Laboratory for Nuclear Science and Physics Department, Massachusetts Institute of Technology, Cambridge, Massachusetts 02139

and

Kyungsik Kang and Chung-I Tan
Department of Physics, Brown University, Providence, Rhode Island 02912

and

J. H. Weis
Laboratory for Nuclear Science and Physics Department, Massachusetts Institute of Technology, Cambridge, Massachusetts 02139

(Received 21 January 1971)

Following Mueller, we relate the single-particle production cross section for the process $a+b\to x+$anything to a discontinuity of the six-line amplitude $a+b+\bar{x}\to a+b+\bar{x}$. Using the dual-resonance model for the six-line amplitude, we obtain an explicit form for the production cross section at high energies. The formula exhibits the expected features of limiting fragmentation, an invariant central region, and triple-Regge asymptotic behavior. In addition, it has a universal cutoff in transverse momentum of the form $e^{-4bp_\perp^2}$ in the central region, where b is the universal trajectory slope. We discuss for particle production some general consequences of duality in the missing mass. For example, we relate the behavior of two-body scattering amplitudes at wide angles to the transverse-momentum dependence of production cross sections. Finally, we discuss the possible experimental relevance of our results.

I. INTRODUCTION

Despite their phenomenological shortcomings, dual-resonance models[1] (DRM) have proven to be an extremely valuable theoretical laboratory for investigating the consequences for scattering amplitudes of the requirements of analyticity, crossing, and Regge asymptotic behavior in the absence of constraints imposed by unitarity. It is remarkable that two-body DRM scattering amplitudes possess such phenomenologically plausible high-energy features as narrow forward peaks and an exponential decrease at fixed wide angles, even though achieving thorough agreement with experiment seems to be impractical.[2]

Mueller[3] has discovered an ingenious method for describing single-particle production at high energies in general terms, using Regge-pole phenomenology. He has shown that single-pole dominance in Regge exchanges at high energies leads to a limiting distribution of produced particle momenta, i.e., the distribution has the property of limiting fragmentation,[4] an invariant central region, and triple-Regge behavior.[5] However, the Regge assumption alone does not provide an explicit description of the shape of the limiting distribution, and in particular does not explain the experimentally observed cutoff in transverse momenta. One must look to specific models to explore these questions.

The DRM has the Regge behavior required to produce a limiting distribution. Accordingly, we have applied the DRM to a study of the single-particle distribution.

Let us briefly review Mueller's analysis and the general features of particle production. Mueller's method relates the cross section for the process $a+b\to x+$anything to the appropriate discontinuity (see Sec. II) in the missing-mass variable of the amplitude for the process

$$a+b+\bar{x}\to a+b+\bar{x}. \tag{1.1}$$

We divide the momentum phase space for the production of particle x into three types of regions, appropriate to the single-, double-, and triple-Regge asymptotic limits in the six-point function, and a fourth region corresponding to an asymptotic limit at fixed missing mass (see Fig. 1). These regions are as follows.

(i) Fragmentation regions (single-Regge). In the asymptotic limit appropriate to this region, the momentum of particle x in the rest system of particle a (or b) is held fixed as the energy increases. We call this the fragmentation region for particle a (or b). Single-Regge exchange implies[3] that in the fragmentation region for particle a at high energies, the number density of particle x, defined as the production cross section divided by the total cross section, i.e.,

$$d\rho_{ab}^{x}=d\sigma_{ab}^{x}/\sigma_{ab}, \tag{1.2}$$

approaches a function of the momentum of particle x in the rest system of particle a, independent of the total energy and the identity of particle b, given by

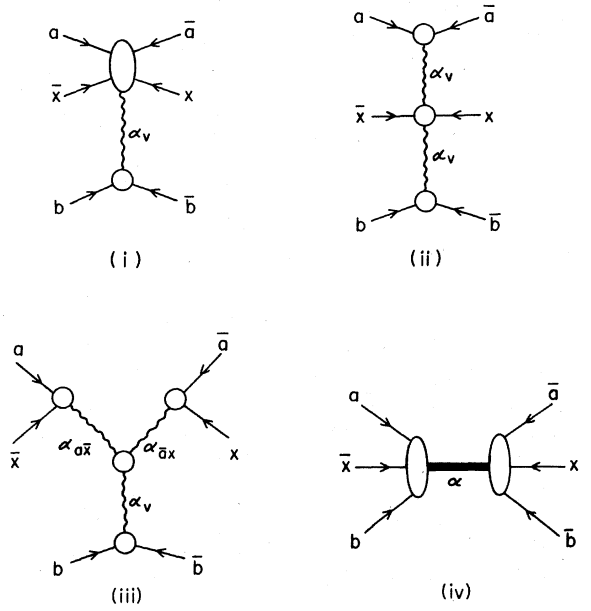

FIG. 1. Diagrams for the six-line amplitude appropriate to the single-Regge (i), double-Regge (ii), triple-Regge (iii), and fixed-missing-mass (iv) asymptotic limits.

$$d\rho_{ab}^{x}=f_a^x(p_\perp,p_\parallel)d^3p/E_x, \tag{1.3}$$

where (E_x,p) is the four-momentum of particle x. A corresponding statement applies in the fragmentation region for particle b.

(ii) Central region (double-Regge). In the asymptotic limit appropriate to this region the transverse momentum of particle x is fixed in any frame of reference that moves parallel to the beam, while the momentum transferred from both a to x and b to x grows. Double-Regge exchange implies[3] that in the central region the number density of particle x approaches a function of the transverse momentum of particle x, independent of the total energy and of particles a and b:

$$d\rho_{ab}^{x}=f^x(p_\perp)d^3p/E_x. \tag{1.4}$$

(iii) Triple-Regge region. Let us construct the invariants from the momenta for particles a, b, and x, as follows:

$$\left.\begin{aligned} s_{a\bar{x}}&=(p_x-p_a)^2,\\ s_{b\bar{x}}&=(p_x-p_b)^2,\end{aligned}\right\}\ \text{momentum transfers}$$
$$s_{ab}=(p_a+p_b)^2,\ \text{total energy} \tag{1.5}$$
$$M^2=(p_a+p_b-p_x),\ \text{missing mass.}$$

The triple-Regge form applies when both s/M^2 and M^2 are large with $s_{a\bar{x}}$ (or $s_{b\bar{x}}$) fixed. This is a region near the phase-space boundary for fixed transverse momenta, but not so close at a particular total energy that the missing mass is too small. We may write[5] the number density in the triple-Regge region for particle a as

$$d\rho_{ab}^{x}=(M^2/s_{ab})^{\alpha_V(0)-2\alpha(s_{a\bar{x}})}h_a^x(s_{a\bar{x}})d^3p/E_x, \tag{1.6}$$

where $\alpha(s_{a\bar{x}})$ is the leading trajectory coupling to $a\bar{x}$ and $\alpha_V(0)$ is the intercept of the leading trajectory coupling to $b\bar{b}$. A corresponding expression applies in the triple-Regge region for particle b. The triple-Regge form (1.6) is most compactly expressed in terms of the invariants, but may also be written in terms of $p_\perp$ and $p_\parallel$ in the rest frame of a, since for large s_{ab}, these are functions of M^2/s_{ab} and $s_{a\bar{x}}$ (see Sec. II).

Both the triple-Regge region and the central region can be regarded as special limits of the fragmentation regions. In the DRM the asymptotic limits can be taken in any order, so that the transition among the various regions is smooth.

We have derived (Sec. III and Appendix A) the distribution functions f_a^x, f_b^x, h_a^x, h_b^x, and f^x in the DRM. Perhaps the most striking feature of our distributions is a universal exponential cutoff at large transverse momentum of the form $e^{-4p_\perp^2}$ in the central region. Transverse momenta are also limited in the fragmentation region. Such a restriction on transverse momenta in high-energy

collisions is a familiar experimental result. We believe the predicted cutoff is a general consequence of Regge asymptotic behavior, crossing, and analyticity, having the same qualitative validity as the narrow forward peak and wide-angle behavior of the two-body DRM amplitudes.

(iv) The region of fixed missing mass. This region is an elliptical ring in the phase space of p. As the energy increases it moves towards the phase-space boundary. In this region the standard phenomenology of four-line amplitudes applies.

It is important to observe that four-line phenomenology gives an alternative dual approach to obtaining the distribution functions. Although this observation can be shown to have validity independent of the specific DRM, let us describe it in somewhat more detail in that model.[6] The missing-mass spectrum is then a discrete set of narrow resonances at $\alpha(M^2)=N$. The contribution to the limiting distribution from a resonance with large N agrees closely with the distribution obtained from Regge behavior described in (i)–(iii). This is analogous to the result for the four-line amplitude that the residue of the Nth pole has the behavior $N^{\alpha(t)}$ for large N, agreeing with the discontinuity in energy of the leading Regge behavior. As the total energy increases the ellipse corresponding to a given resonance moves towards the phase-space boundary. Thus we see that for sufficiently large N, the contribution from a given resonance traces out the *entire* limiting distribution as the total energy is increased.[7] Of course, how large N must be may depend upon the region of phase space under consideration.

This result is a particularly useful application of general dual principles, since it relates the energy and angle variations of differential cross sections for $a+b\to x+M^2$ for fixed resonant mass to the limiting distribution for the production of particle x. For example, it suggests that in general it may be possible to relate the observed exponential cutoff in $p_\perp$ in production distributions to the behavior near threshold at fixed angle and large resonant mass in differential cross sections. We will discuss these observations in greater detail in Sec. IV and Appendix B.

In the concluding section we discuss some problems in reconciling our results with unitarity in the DRM.

II. GENERAL CONSIDERATIONS

After establishing our notation, we discuss the generalized optical theorem, the kinematics of the regions (i)–(iii) above, and the dual diagrams which contribute in these regions.

A. Notation, Optical Theorem, and Kinematics

We find it convenient to use an all-incoming convention for particle momenta (see Fig. 2). The momenta p_a $(=-p_{\bar a})$ and p_b $(=-p_{\bar b})$ are thus positive timelike, whereas $p_{\bar x}$ $(=-p_x)$ is negative timelike. The invariants of interest are

$$M^2=(p_a+p_b+p_{\bar x})^2, \quad \text{missing mass}$$

$$s_{ab}=(p_a+p_b)^2, \quad \text{total energy}$$

$$\left.\begin{aligned} s_{a\bar x}&=(p_a+p_{\bar x})^2,\\ s_{b\bar x}&=(p_b+p_{\bar x})^2,\end{aligned}\right\} \quad \text{momentum transfers.}$$

With our conventions, in the physical region of interest, variables with two unbarred or barred labels are positive "energy" variables and those with one unbarred and one barred label are negative "momentum transfer" variables.

The "correct" discontinuity in the missing-mass variable is the one which gives the sum over intermediate states of the modulus squared of the production amplitudes. There are four variables in the forward six-line amplitude, which have normal thresholds in the physical region for the process $a+b\to x+M^2$. These are s_{ab} and $s_{\bar a\bar b}$ (the incoming and outgoing total energies), $M^2\equiv s_{ab\bar x}$, and s_{abx}

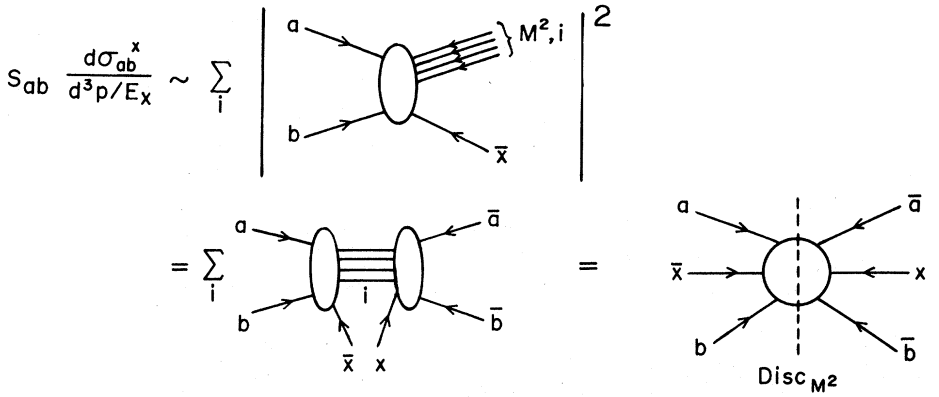

FIG. 2. Kinematics and optical theorem.

(the "crossed-energy" variable). We have not studied the prescription for taking the correct discontinuity for a general amplitude. In the case of the DRM we find that amplitudes containing singularities in the variable s_{abx} do not contribute to the asymptotic limits, so we ignore these singularities. The correct discontinuity is then obtained by encircling only the singularities in M^2, keeping s_{ab} fixed above and $s_{\bar{a}\bar{b}}$ fixed below their respective singularities. This will have important consequences in what follows.

Since we are interested in the limiting single-particle production distribution we will be considering in general the limit

$$s_{ab} \to +\infty + i\epsilon, \quad s_{\bar{a}\bar{b}} \to +\infty - i\epsilon, \quad \text{and} \quad M^2 \to +\infty \pm i\epsilon. \tag{2.1}$$

Furthermore, in the various kinematic regions discussed in Sec. I, we have[8]

(i) Fragmentation of a:

$$s_{b\bar{x}} \to -\infty \tag{2.2}$$

with $s_{a\bar{x}}$, s_{ab}/M^2 fixed. This is equivalent to fixing the momentum of x in the rest frame of a, since

$$s_{a\bar{x}} = m_a^2 + m_x^2 - 2m_a E_x$$

and

$$s_{ab}/M^2 = [1 - (E_x - p_{\parallel})/m_a]^{-1}. \tag{2.3}$$

Fragmentation of b:

$$s_{a\bar{x}} \to -\infty \tag{2.2$'$}$$

with $s_{b\bar{x}}$, s_{ab}/M^2 fixed.

(ii) Central region:

$$s_{a\bar{x}},\ s_{b\bar{x}} \to -\infty \tag{2.4}$$

with $s_{a\bar{x}} s_{b\bar{x}}/s_{ab} \equiv \kappa$ fixed. One finds in this limit the important relation

$$\kappa = p_{\perp}^2 + m_x^2. \tag{2.5}$$

(iii) Phase-space boundary of fragmentation regions: In addition to (2.2) or (2.2$'$), we have

$$s_{ab}/M^2 \to +\infty. \tag{2.6}$$

Of course, the corresponding limits are simultaneously taken with $s_{\bar{a}\bar{b}}$, $s_{\bar{a}x}$, $s_{\bar{b}x}$.

B. Dual-Resonance Model

In the usual DRM for the six-point function[9] there are contributions from $\frac{1}{2}(6-1)! = 60$ distinct diagrams corresponding to the different permutations of the external lines. However, we shall see that only seven of these contribute to the limiting single-particle-production distribution.

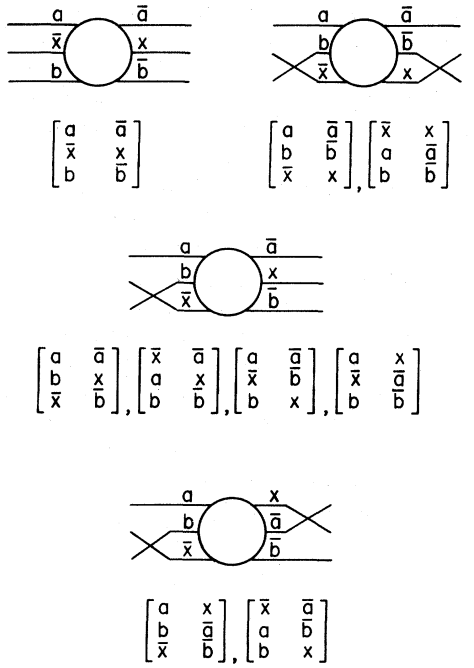

FIG. 3. Four classes of diagrams contributing to Disc_{M^2}.

Only the 18 diagrams which have a, b, and $\bar{x}$ adjacent can contribute to the discontinuity in the $ab\bar{x}(M^2)$ channel. These 18 can be grouped into eight topological classes. In Fig. 3 we show four of the classes; the other four classes are obtained by inverting the order of the three lines on one side of the diagram; for example,

$$\begin{bmatrix} a & \bar{a} \\ \bar{x} & x \\ b & \bar{b} \end{bmatrix} \to \begin{bmatrix} b & \bar{a} \\ \bar{x} & x \\ a & \bar{b} \end{bmatrix}.$$

For visual clarity we have introduced the notation

$$\begin{bmatrix} u & z \\ v & y \\ w & x \end{bmatrix} \equiv B_6(p_u, p_v, p_w, p_x, p_y, p_z),$$

which, for typographical convenience, we shall write in text material as $\left[\begin{smallmatrix} z & y & x \\ u & v & w \end{smallmatrix}\right]$.

Only the first three classes of diagrams in Fig. 3, consisting of a total of seven distinct diagrams, contribute to the limiting distributions. To see this we use the symmetry properties of the dual amplitudes discovered by Plahte.[10] Using these properties we can express each of the 18 diagrams as a simple multiplicative factor times any given single diagram with some trajectory intercepts modified. Thus, we have as representative results,[11]

$$\mathrm{Disc}_{M^2}\begin{bmatrix} a & \bar{a} \\ b & \bar{b} \\ \bar{x} & x \end{bmatrix} = \frac{\sin\pi(\alpha_{ab} + \alpha_{b\bar{x}} - \alpha_{ab\bar{x}})\sin\pi(\alpha_{\bar{a}\bar{b}} + \alpha_{b\bar{x}} - \alpha_{\bar{a}\bar{b}x})}{\sin\pi(\alpha_{ab} - \alpha_{ab\bar{x}})\sin\pi(\alpha_{\bar{a}\bar{b}} - \alpha_{\bar{a}\bar{b}x})} \mathrm{Disc}_{M^2}\begin{bmatrix} a & \bar{a} \\ \bar{x} & x \\ b & \bar{b} \end{bmatrix}, \tag{27a}$$

$$\mathrm{Disc}_{M^2}\begin{bmatrix} a & \bar{a} \\ b & x \\ \bar{x} & \bar{b} \end{bmatrix} = \frac{\sin\pi(\alpha_{ab}+\alpha_{b\bar{x}}-\alpha_{ab\bar{x}})}{\sin\pi(\alpha_{ab}-\alpha_{ab\bar{x}})}\,\mathrm{Disc}_{M^2}\begin{bmatrix} a & \bar{a} \\ \bar{x} & x \\ b & \bar{b} \end{bmatrix}, \tag{2.7b}$$

$$\mathrm{Disc}_{M^2}\begin{bmatrix} b & \bar{a} \\ \bar{x} & x \\ a & \bar{b} \end{bmatrix} = \frac{\sin\pi(\alpha_{ab\bar{x}}-\alpha_{a\bar{x}}-\alpha_{b\bar{x}})\sin\pi(-\alpha_{a\bar{x}})\sin\pi(-\alpha_{b\bar{x}})}{\sin\pi(\alpha_{ab\bar{x}}-\alpha_{a\bar{x}})\sin\pi(\alpha_{ab\bar{x}}-\alpha_{b\bar{x}})\sin\pi(-\alpha_{a\bar{x}}-\alpha_{b\bar{x}})}\,\mathrm{Disc}_{M^2}\begin{bmatrix} a & \bar{a} \\ \bar{x} & x \\ b & \bar{b} \end{bmatrix}. \tag{2.7c}$$

To derive the above expressions we have used Plahte's linear relationships [see his Eq. (3.3)]. In general, for the six-point function these are relationships between five different diagrams, but taking the discontinuity reduces them to relationships among three diagrams, which in turn can be reduced to relationships between pairs of diagrams by taking imaginary parts. The sine factors are very easily obtained in this way. Determining the modifications of the trajectory intercepts requires some labor but fortunately is irrelevant to what follows.

The importance of Eqs. (2.7) and their analogs is that they relate all the diagrams to $\mathrm{Disc}_{M^2}\left[\begin{smallmatrix} \bar{a} & x & \bar{b} \\ a & \bar{x} & b \end{smallmatrix}\right]$. In the asymptotic regions of interest [Eqs. (2.1)–(2.6)], the standard integral representation for this function is defined and the function is real. The sine factors thus contain all the information on the phases of the diagrams. As they stand these factors are infinitely oscillating and do not have a well-defined asymptotic limit. To give meaning to the asymptotic limit along rays in complex α_{ab}, $\alpha_{a\bar{x}}$, and $\alpha_{b\bar{x}}$, we adopt a phase convention, fixing the phases of α_{ab}, $-\alpha_{a\bar{x}}$, $-\alpha_{b\bar{x}}$ (and $\alpha_{\bar{a}\bar{b}}$, $-\alpha_{\bar{a}x}$, $-\alpha_{\bar{b}x}$) to have the same sign when they are asymptotic. This choice of phases will be justified further in Sec. IV. We only remark here that the same problem arises in defining the asymptotic behavior of the four-point function at fixed momentum transfer[12] or fixed scattering angle at high energy.[13]

With the above phase convention it is straightforward to verify that the diagrams contribute in the various kinematic regions as follows:

(i) Fragmentation of a:

$$\begin{bmatrix} a & \bar{a} \\ \bar{x} & x \\ b & \bar{b} \end{bmatrix}, \quad \begin{bmatrix} \bar{x} & \bar{a} \\ a & x \\ b & \bar{b} \end{bmatrix}, \quad \begin{bmatrix} a & x \\ \bar{x} & \bar{a} \\ b & \bar{b} \end{bmatrix}, \quad \begin{bmatrix} \bar{x} & x \\ a & \bar{a} \\ b & \bar{b} \end{bmatrix}. \tag{2.8a}$$

Fragmentation of b:

$$\begin{bmatrix} a & \bar{a} \\ \bar{x} & x \\ b & \bar{b} \end{bmatrix}, \quad \begin{bmatrix} a & \bar{a} \\ b & x \\ \bar{x} & \bar{b} \end{bmatrix}, \quad \begin{bmatrix} a & \bar{a} \\ \bar{x} & \bar{b} \\ b & x \end{bmatrix}, \quad \begin{bmatrix} a & \bar{a} \\ b & \bar{b} \\ \bar{x} & x \end{bmatrix}. \tag{2.8b}$$

(ii) Central Region:

$$\begin{bmatrix} a & \bar{a} \\ \bar{x} & x \\ b & \bar{b} \end{bmatrix}. \tag{2.8c}$$

The contributions of diagrams other than the ones listed vanish exponentially due to the sine factors when the variables are taken to infinity in the complex plane. The fact that the diagrams contribute as shown above is very satisfying, since they are precisely the ones which have the required Regge behaviors to produce limiting distributions according to Mueller's analysis [see Sec. I (i)–(iii)]. Thus, for example, the four diagrams contributing to the fragmentation of a are the only four diagrams with Regge trajectories in the $b\bar{b}$ channel. (Note that these diagrams provide the signature factors for the Regge trajectories in the $a\bar{x}$ and $\bar{a}x$ channels entering in the triple-Regge vertex, since the sine factors reduce to the usual Regge phases.) Also, only one diagram of the 18 has the required double-Regge behavior and it is the only one we find contributing in the central region.

III. LIMITING DISTRIBUTIONS

In this section we present and discuss the explicit expressions for the limiting distributions [Eqs. (1.3), (1.4), and (1.6)] in the DRM. The derivations are given in Appendix A.

We assume the standard form for the dual six-point function.[9] Thus, for example,

$$\begin{bmatrix} a & \bar{a} \\ \bar{x} & x \\ b & \bar{b} \end{bmatrix} = \int_0^1\int_0^1\int_0^1 dx_1dx_2dy\,x_1^{-\alpha_{b\bar{x}}-1}(1-x_1)^{-\alpha_{a\bar{x}}-1}x_2^{-\alpha_{\bar{b}x}-1}(1-x_2)^{-\alpha_{\bar{a}x}-1}y^{-\alpha-1}(1-y)^{-\alpha_{a\bar{a}}-1}$$

$$\times(1-x_1y)^{-\alpha_{a\bar{a}\bar{x}}+\alpha_{a\bar{x}}+\alpha_{a\bar{a}}}(1-x_2y)^{-\alpha_{a\bar{a}x}+\alpha_{\bar{a}x}+\alpha_{a\bar{a}}}(1-x_1x_2y)^{-\alpha_{a\bar{a}}-\alpha_{b\bar{b}}+\alpha_{a\bar{a}\bar{x}}+\alpha_{a\bar{a}x}}, \tag{3.1}$$

where[14,15]

$$\alpha = M^2 + a, \quad \alpha_{ab} = s_{ab} + a_{ab}, \quad \alpha_{a\bar{x}} = s_{a\bar{x}} + a_{a\bar{x}}, \text{ etc.} \tag{3.2}$$

(i) Fragmentation Region. In the fragmentation region for b we obtain directly from Eq. (A3) and the definitions (1.2) and (1.3) the contribution of $\left[\begin{smallmatrix}\bar{a} & x\\ a & \bar{x}\end{smallmatrix}\begin{smallmatrix}\bar{b}\\ b\end{smallmatrix}\right]$ as follows:

$$f_b^x(p_\perp, p_\parallel) = \left(\frac{\alpha}{\alpha_{ab}}\right)^{\alpha_V}\left(-\frac{\alpha_{a\bar{x}}}{\alpha}\right)^{\alpha_{b\bar{x}}}\left(-\frac{\alpha_{\bar{a}x}}{\alpha}\right)^{\alpha_{\bar{b}x}}$$
$$\times\int_0^\infty\int_0^\infty dy_1 dy_2\,\theta(1-y_1-y_2)\,y_1^{-\alpha_{b\bar{x}}-1}y_2^{-\alpha_{\bar{b}x}-1}\left(1-\frac{\alpha}{\alpha_{a\bar{x}}}y_1\right)^{\alpha_{b\bar{x}}+\alpha_{b\bar{b}}-\alpha_{a\bar{a}x}}$$
$$\times\left(1-\frac{\alpha}{\alpha_{\bar{a}x}}y_2\right)^{\alpha_{\bar{b}x}+\alpha_{b\bar{b}}-\alpha_{a\bar{a}\bar{x}}}\left(1-\frac{\alpha}{\alpha_{a\bar{x}}}y_1-\frac{\alpha}{\alpha_{\bar{a}x}}y_2\right)^{-\alpha_V-\alpha_{b\bar{b}}+\alpha_{a\bar{a}x}+\alpha_{a\bar{a}\bar{x}}}(1-y_1-y_2)^{\alpha_V}. \tag{3.3}$$

From

$$\frac{\alpha}{\alpha_{ab}}=\frac{M^2}{s_{ab}},\quad \frac{\alpha_{a\bar{x}}}{\alpha}=1-\frac{s_{ab}}{M^2},\ \text{and}\ \frac{\alpha_{\bar{a}x}}{\alpha}=1-\frac{s_{\bar{a}\bar{b}}}{M^2} \tag{3.4}$$

and the analog of (2.3), we see that f_b^x is a function of the required variables ($p_\perp$ and $p_\parallel$). In obtaining (3.3) we have assumed $\alpha_{a\bar{a}}=\alpha_V$, where α_V is the trajectory dominating in the total cross section

$$\sigma_{ab}=\frac{\pi}{\Gamma(\alpha_V+1)}\alpha_{ab}{}^{\alpha_V-1}. \tag{3.5}$$

This natural assumption is necessary to obtain a finite limiting distribution. As discussed in Sec. V, we feel that the most realistic choice for α_V in our model is the P' trajectory.

The contributions to f_b^x of the other three terms can be obtained by permuting b and $\bar{x}$ and/or $\bar{b}$ and x in (3.3) [except in the first factor $(\alpha/\alpha_{ab})^{\alpha_V}$] and thus have a very similar form.

Near the phase-space boundary, i.e., the triple-Regge region (iii), we have from (3.3) and the relation $M^2+m_a{}^2+m_b{}^2+m_x{}^2=s_{ab}+s_{a\bar{x}}+s_{b\bar{x}}$,

$$f_b^x \underset{s_{ab}/M^2\to\infty}{\sim}\left(\frac{M^2}{s_{ab}}\right)^{\alpha_V}\left(\frac{s_{ab}}{M^2}\right)^{\alpha_{b\bar{x}}}\left(\frac{s_{\bar{a}\bar{b}}}{M^2}\right)^{\alpha_{\bar{b}x}}\int_0^\infty\int_0^\infty dy_1dy_2\,\theta(1-y_1-y_2)y_1^{-\alpha_{b\bar{x}}-1}y_2^{-\alpha_{\bar{b}x}-1}(1-y_1-y_2)^{\alpha_V}.$$

Performing the integration explicitly and observing the phase definition (2.1), we find for the *sum* of the four diagrams[16]

$$h_b^x=(1+\tau_{b\bar{x}}e^{-i\pi\alpha_{b\bar{x}}})(1+\tau_{\bar{b}x}e^{i\pi\alpha_{\bar{b}x}})\frac{\Gamma(-\alpha_{b\bar{x}})\Gamma(-\alpha_{\bar{b}x})\Gamma(\alpha_V+1)}{\Gamma(-\alpha_{b\bar{x}}-\alpha_{\bar{b}x}+\alpha_V+1)}. \tag{3.6}$$

From (3.6) we see clearly that the opposite phases of s_{ab} and $s_{\bar{a}\bar{b}}$ are necessary to insure the reality of h_b^x.

Expressions for f_a^x and h_a^x can be obtained by interchanging a ($\bar{a}$) and b ($\bar{b}$) in the above.

(ii) Central Region. As discussed in Sec. II, f_x gets a contribution only from the diagram $\left[\begin{smallmatrix}\bar{a} & x\\ a & \bar{x}\end{smallmatrix}\begin{smallmatrix}\bar{b}\\ b\end{smallmatrix}\right]$. From the definitions (1.2) and (1.4) and the results (A8) and (3.5), we have

$$f^x(p_\perp)=\frac{\Gamma(\alpha_V+1)}{\pi}\kappa^{\alpha_V}\int_0^1 dz\,z^{-\alpha_{a\bar{a}x}-1}(1-z)^{-\alpha_{a\bar{a}\bar{x}}-1}\left[\mathrm{Disc}_x\mathcal{V}\left(\alpha_V,\alpha_V;x=\frac{\kappa}{z(1-z)}\right)\right], \tag{3.7}$$

where $\kappa=p_\perp{}^2+m_x{}^2$. In (3.7), $\mathcal{V}$ is the usual two-Reggeon–single-particle vertex[17]:

$$\mathcal{V}(\alpha_1,\alpha_2;x)=\int_0^\infty\int_0^\infty dy_1dy_2y_1^{-\alpha_1-1}y_2^{-\alpha_2-1}\exp\left(-y_1-y_2+\frac{y_1y_2}{x}\right). \tag{3.8}$$

In order to obtain the finite limiting distribution (3.7), we have made the natural assumption that $\alpha_{a\bar{a}}=\alpha_{b\bar{b}}=\alpha_V$.

As $p_\perp{}^2\sim\kappa\to\infty$, f^x has the behavior

$$f^x(p_\perp)\underset{p_\perp\to\infty}{\sim}\sqrt{\pi}\,\Gamma(\alpha_V+1)2^{\alpha_{a\bar{a}x}+\alpha_{a\bar{a}\bar{x}}-4\alpha_V-2}(p_\perp)^{-2\alpha_V-3}e^{-4p_\perp{}^2}. \tag{3.9}$$

The distribution has a remarkable exponential cutoff in transverse momentum, restricting $p_\perp{}^2$ to values around $\frac{1}{4}$ (GeV/c)^2, in qualitative agreement with experiment.

We have computed the function f^x to study its behavior at low values of $p_\perp{}^2$ and to make a cursory comparison with experiment.

We plot the function f^x for two choices for the intercept α_V in Fig. 4 and two choices of the mass of the produced particle in Fig. 5 (for a trajectory slope of 1/GeV^2). The curves are normalized to unit area.

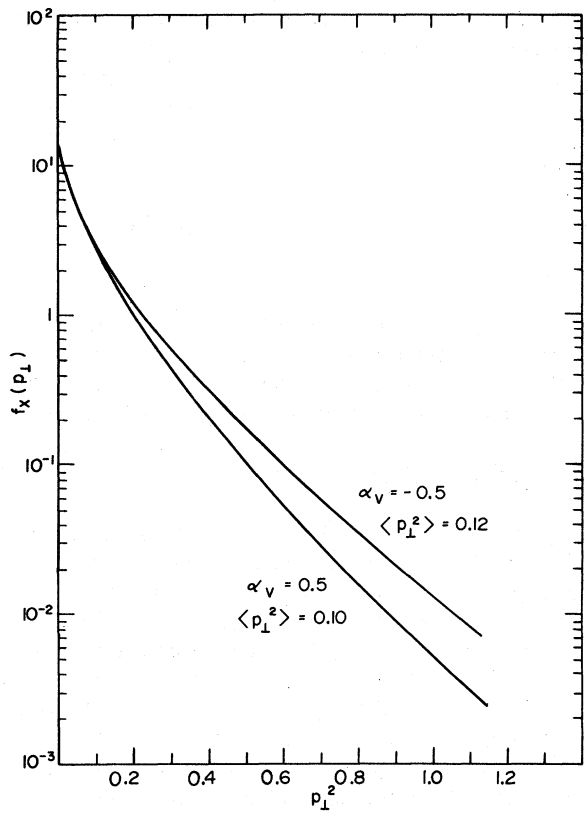

FIG. 4. Transverse momentum distribution for particle production in the central region for particle mass squared 0.02 and vacuum trajectory intercepts −0.5 and 0.5. The curves are normalized to unit area.

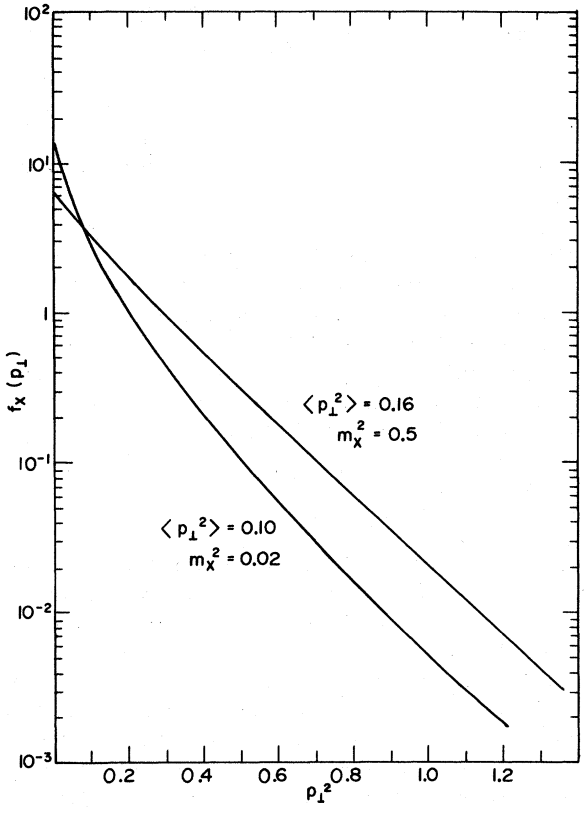

FIG. 5. Transverse momentum distribution for particle production in the central region for particle mass squared 0.02 and 0.5 and vacuum trajectory intercept 0.5. The curves are normalized to unit area.

We find that for $\alpha_V = 0.5$, a value which we prefer (see Sec. V), the average value of $p_\perp{}^2$ for $m_x{}^2 = 0.02$ is $\langle p_\perp{}^2 \rangle = 0.10$. This value is determined more by the sharpness of the low-$p_\perp{}^2$ distribution that the asymptotic behavior $e^{-4p_\perp{}^2}$. As shown in Fig. 4 the distribution is less sharp for lower intercepts. This is suggested by the asymptotic form (3.9). The distribution is also less sharp for larger masses (Fig. 5). For $m_x{}^2 = 0.5$, $\langle p_\perp{}^2 \rangle = 0.16$. The average values of $\langle p_\perp \rangle$ for $m_x{}^2 = 0.02$ and 0.5 are 260 and 360 MeV/c, respectively, with $\alpha_V = 0.5$. The distribution for $m_x{}^2 = 1.0$ (not shown) differs only slightly from the distribution for $m_x{}^2 = 0.5$. Figures 4 and 5 were calculated with $\alpha_{a\bar{a}x} = \alpha_{a\bar{a}\bar{x}} = 0$, but they depend only weakly upon this parameter as might be expected from Eq. (3.7). We have not studied the $p_\parallel$ dependence of the transverse momentum distribution in the fragmentation region.

Experimentally, the momentum distributions are quite a bit broader.[18] Average values of $p_\perp$ for pions range from 300 to 500 MeV/c and the distributions fall off less rapidly at large $p_\perp{}^2$. Crabb *et al.*[19] report an exponential falloff of $e^{-2.7p_\perp{}^2}$ for the π^+ distribution in the range $1 < p_\perp{}^2 < 4\,(\mathrm{GeV}/c)^2$, an exponential rate slightly greater than half of ours for this range. Nevertheless, considering the limitations of the model, chiefly its neglect of unitarity, we find the qualitative resemblance to experimental distributions to be quite impressive.

IV. DUALITY

A consequence of duality for the four-line DRM amplitude is the following: The discontinuity of the amplitude near the pole at $\alpha_s = N$ behaves like

$$\mathrm{Disc}B(-\alpha_s, -\alpha_t) \approx \pi \frac{\Gamma(\alpha_t + N + 1)}{\Gamma(N+1)\Gamma(\alpha_t + 1)} \delta(\alpha_s - N),$$

which for large N is

$$\sim \frac{\pi N^{\alpha_t}}{\Gamma(\alpha_t + 1)} \delta(\alpha_s - N). \tag{4.1}$$

On the other hand, the discontinuity of the Regge asymptotic form is

$$\mathrm{Disc}\Gamma(-\alpha_t)(-\alpha_s)^{\alpha_t} = \frac{\pi s^{\alpha_t}}{\Gamma(\alpha_t+1)}\,. \tag{4.2}$$

Clearly the integrals over (4.1) and (4.2) from $\alpha_s = N - \frac{1}{2}$ to $\alpha_s = N + \frac{1}{2}$ are very nearly equal.

In the same way for sufficiently large N the narrow resonances in M^2 in the six-point function will give a good approximation to the Regge behaviors (i)–(iii) and thus the distributions given in Sec. III.[20] Each such resonance corresponds in the phase space of particle x to an ellipse which for zero width is a δ function with a weight equal to the differential cross section for producing the resonance. In the center-of-mass system of a and b, the ellipse is a circle of radius

$$p = \frac{\lambda^{1/2}(M^2, s_{ab}, m_x^2)}{2\sqrt{s_{ab}}}\,,$$

where λ is the usual symmetric function (see Fig. 6). Thus, if N is large enough, we expect the limiting distributions to agree with the resonance contributions on the average.

As the total energy s_{ab} is increased, each given resonance ellipse moves toward the boundary and new ellipses appear at the center. From the above discussion we thus expect each ring to trace out an approximation to the complete limiting distribution as it moves from the center to the edge. Thus one might hope to obtain the full distribution from an experiment at one fixed missing mass. The question is, of course, how large that missing mass must be. We discuss this question in general terms below.

In Fig. 6 we have indicated the regions near the boundary of phase space which correspond to the Regge and fixed-angle behaviors of the four-line amplitudes. Consider first the Regge behavior of $a+b \to x+M^2$ at fixed $s_{a\bar{x}}$. A given narrow resonance at $\alpha = N$ gives a contribution

$$\frac{d\rho_{ab}^x}{d^3p/E_x} \approx \frac{1}{\beta_{a\bar{a}}\, s_{ab}^{\alpha_V} \beta_{b\bar{b}}} |\beta_{a\bar{x}}\, s_{ab}^{\alpha_{a\bar{x}}} \beta_{bN}|^2 \delta(\alpha - N). \tag{4.3}$$

This Regge behavior should hold if $s_{ab} \gg N$. If a limiting distribution is approached in the fragmentation region of a, (4.3) must become a function of the nonasymptotic variables s_{ab}/N and $s_{a\bar{x}}$; thus

$$\frac{d\rho_{ab}^x}{d^3p/E_x} \approx \left(\frac{s_{ab}}{N}\right)^{2\alpha_{a\bar{x}} - \alpha_V} h_a'(\alpha_{a\bar{x}})\, \delta(\alpha - N), \tag{4.4}$$

which agrees with (1.6).[21] Thus the assumptions of duality, two-two Regge behavior, and existence of a limiting distribution imply the triple-Regge behavior. We note that the Regge behavior $(M^2)^{\alpha_V}$ in the six-line amplitude is responsible for the term $(M^2/s_{ab})^{\alpha_V}$ in the triple-Regge analysis. It is therefore expected that the resonances in M^2 will reproduce this behavior only for large N.[20, 22] We remark that the narrowness of the forward peak should be correlated with the concentration of the single-particle spectrum around small values of $p_\perp$ in this region.

The behavior in the remaining phase space is associated with the fixed-angle behavior of the two-two amplitudes. Experimentally, two-body cross sections fall exponentially in energy at fixed angle

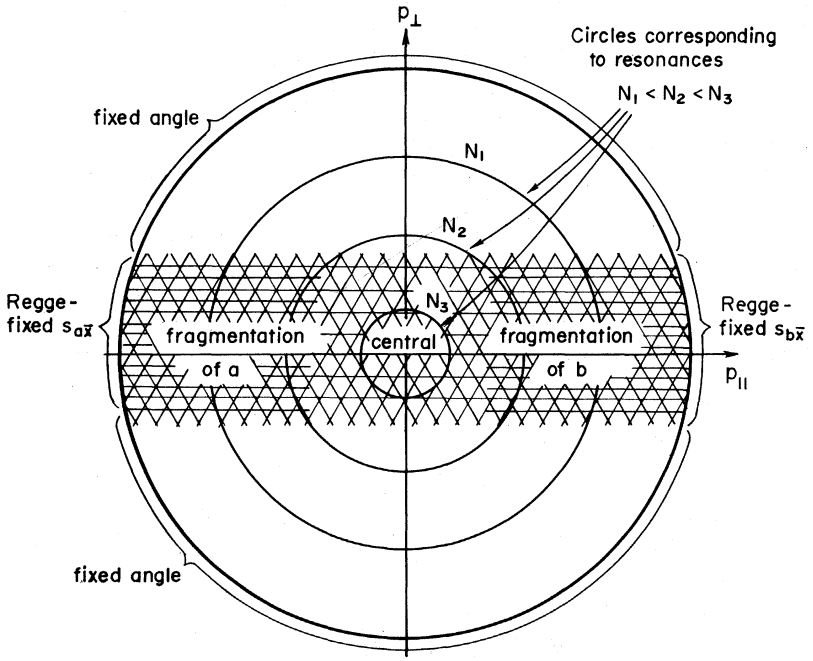

FIG. 6. Center-of-mass momentum phase space for particle x at a given s_{ab}. The regions indicated on the boundary are the appropriate regions of the four-line amplitude.

($\neq 0°, 180°$). One might expect that this explains at once the experimentally observed limitation on transverse momenta. However, it must be borne in mind that the central region of the limiting distribution is a region of high M^2 with $s \approx M^2$, i.e., energies *near the threshold* for producing the missing-mass resonance, rather than with $s \gg M^2$, i.e., far from threshold, as is conventionally meant by asymptotic behavior at fixed angle. In the absence of applicable experimental data we return to the DRM to study the relationship between the asymptotic behavior near threshold and far from threshold at fixed angles and large missing mass. The behavior is in fact somewhat different. At $p_{\parallel}^{\text{c.m.}} = 0$, the behavior near threshold is $e^{-4p_\perp{}^2}$, agreeing with the limiting distribution, whereas for $s \gg M^2$ it is $e^{-(8\ln 2)p_\perp{}^2}$. To study further the relationship between these behaviors we have examined the simpler case of the five-point function for $a+b \to a+\bar{x}+b$, where the corresponding behaviors are $e^{-p_\perp{}^2}$ and $e^{-(4\ln 2)p_\perp{}^2}$. The results of a calculation of $g_N(p_\perp)$ [corresponding to $f(p_\perp)$] for various N is shown in Fig. 7.

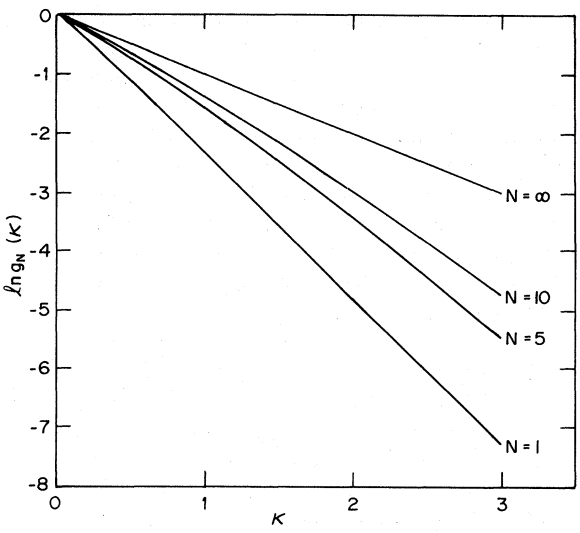

FIG. 7. Plot based upon the five-point dual-resonance model, illustrating the rate at which contributions from various resonance cross sections approach the limiting curve. The curves for resonance spins $N = 1$, 5, and 10 are shown. The limiting curve is $N = \infty$.

Each curve has a gradually increasing logarithmic slope c in $e^{-cp_\perp{}^2}$. For $N = 1$, the wide-angle slope $c = 4\ln 2$ has practically been reached at $\kappa = 1$, but for $N = 10$, there is only a small departure from $c = 1$. The deviations are consistent with a theoretical evaluation of the correction to $c = 1$ in this model, i.e.,

$$c = 1 + (\kappa/N)^{1/2} + O(\kappa/N).$$

Although the $s \gg M^2$ fixed-angle behavior does not explain the limitation in transverse momenta, we find the existence of the two different exponential behaviors very intriguing.

Finally, we return to the important question of the definition of phases in Eq. (2.7). Consider for simplicity the residue of the lowest pole in M^2 in the six-point function ($N = 0$). Similar arguments apply to higher poles. The full residue for the sum of all permutations[16] is

$$[B(-\alpha_{a\bar{x}}, -\alpha_{b\bar{x}}) + B(-\alpha_{ab}, -\alpha_{a\bar{x}}) + B(-\alpha_{ab}, -\alpha_{b\bar{x}})][B(-\alpha_{\bar{a}x}, -\alpha_{\bar{b}x}) + B(-\alpha_{\bar{a}\bar{b}}, -\alpha_{\bar{a}x}) + B(-\alpha_{\bar{a}\bar{b}}, -\alpha_{\bar{b}x})]$$

$$= \left[1 + \frac{\sin\pi(\alpha_{ab} + \alpha_{a\bar{x}})}{\sin\pi\alpha_{ab}} + \frac{\sin\pi(\alpha_{ab} + \alpha_{b\bar{x}})}{\sin\pi\alpha_{ab}}\right] B(-\alpha_{a\bar{x}}, -\alpha_{b\bar{x}}) \left[1 + \frac{\sin\pi(\alpha_{\bar{a}\bar{b}} + \alpha_{\bar{a}x})}{\sin\pi\alpha_{\bar{a}\bar{b}}} + \frac{\sin\pi(\alpha_{\bar{a}\bar{b}} + \alpha_{\bar{b}x})}{\sin\pi\alpha_{\bar{a}\bar{b}}}\right] B(-\alpha_{\bar{a}x}, -\alpha_{\bar{b}x}), \tag{4.5}$$

where we have suppressed some modifications of trajectory intercepts. We note that the sine factors are undefined unless some choice of phase is made. In the wide-angle region we believe the appropriate choice is to let α_{ab}, $-\alpha_{a\bar{x}}$, $-\alpha_{b\bar{x}}$ (and $\alpha_{\bar{a}\bar{b}}$, $-\alpha_{\bar{a}x}$, $-\alpha_{\bar{b}x}$) have the same phase.[23] Then all the sine factors vanish exponentially. Considering the smooth connection discussed above between the behavior in the central region and at fixed angle, it is especially appropriate to make the same choice of phase in the central region. This again causes the sine factors to vanish exponentially.[24-26]

V. CONCLUSION

Instead of applying the Mueller analysis to the six-line amplitude to construct the production spectrum in the DRM, one could sum explicitly the contributions from multiparticle production, representing the 2-n scattering amplitudes with the DRM. Because the amplitudes are not unitary, one does not expect the results to agree. By the same token, one would not expect the imaginary part of the forward 2-2 amplitude to agree with the sums over the partial cross sections computed from the 2-n amplitudes.

Is it possible then to justify working with the six-line amplitude at all? The work of DiGiacomo *et al.*[27] suggests that the agreement between the two approaches may be better than one might have expected. In their treatment of the DRM, zero-width

resonances are taken to be the limiting case of narrow-width resonances that are explicitly unitary in the Breit-Wigner sense, i.e., the residues of the resonances are taken to be proportional to their widths. With this interpretation, the tree graphs containing direct-channel resonances satisfy unitarity near the direct-channel poles. Thus these authors were led to look elsewhere for "Pomeranchuk" contributions, namely, to contributions from loops arising from trees without direct-channel resonances.

We suggest, however, that such a treatment neglects an important multiperipheral effect in the 2-n amplitudes, which is seen most clearly if one displaces the poles from the real axis. Then the n-particle production amplitudes in the DRM have a multi-Regge asymptotic behavior for large subenergies. If they are approximated in this way, they satisfy the criteria for a multiperipheral model of n-particle production.[28] With an arbitrary choice for the strength of the vertices, it is likely that such amplitudes, when integrated and summed over n, would produce an output pole different from the leading input pole. In the multi-Regge sense, therefore, we suggest that unitarity need not be satisfied by the tree graphs with direct-channel resonances. We agree with DiGiacomo *et al.* that including other graphs is likely to produce a Pomeranchuk effect even when the Pomeranchuk is not incorporated in the tree graphs themselves. We believe that the dual features of the six-point function are best suited for a treatment of "non-Pomeranchuk" effects in production distributions. Therefore, we are justified in using the six-line amplitude only to the extent that, having neglected the Pomeranchuk effects, the results of the two approaches can be made consistent with a judicious choice of the trajectory intercept.

How seriously should one take our results? If one insists upon an experimental application, we suggest that the most realistic choice for the leading vacuum pole in our expressions is the P' trajectory. Since, at sufficiently large energies, the Pomeranchuk trajectory will prevail, our results should apply only at intermediate energies, where the P' still has strength, or in combinations of cross sections which exclude the Pomeranchuk trajectory. However, any experimental application will be hampered, because our expressions inherit the usual difficulties of DRM's. For example, tachyons cause singularities in the fragmentation distribution, and other DRM's beside the one of Ref. 9 can be constructed. We believe, therefore, that our results will be chiefly of theoretical interest. Nevertheless, we suggest that such features of the model as the exponential cutoff in transverse momentum have the same general validity as the high-energy two-body features of narrow forward peaks and an exponential falloff at wide angles; indeed, the coarse agreement with experimental distributions is further indication that the model is qualitatively sound.

Note added. In the final stages of this work we received preprints of two studies independent of our own of single-particle distributions in the dual-resonance model, by Gordon and Veneziano[29] and by Virasoro.[30] Gordon and Veneziano discuss the contributions to single-particle production in the spirit of Ref. 27 and emphasize the importance of loop-type diagrams. They restrict their explicit calculations to the fragmentation regions and obtain results similar to ours, although they do not obtain an explicit form for the discontinuity in M^2, except in the triple-Regge region. Virasoro obtains expressions essentially equivalent to ours for both the fragmentation and central regions for a particular choice of trajectory intercepts and masses. However, on a number of points, particularly on the question of which diagrams contribute in the central region, his interpretation differs from ours. He calculates the contribution of $\left[\begin{smallmatrix}\bar{a} & \bar{b} & x\\ a & b & \bar{x}\end{smallmatrix}\right]$ and notes that this gives a finite contribution in the central region only for particular choices of the trajectory intercepts. His result agrees with ours (Appendix A) if the sine factors are neglected. However, with our interpretation of the sine factors, regardless of the intercepts, the only diagram contributing in the central region is the one that satisfies Mueller's requirement of double-Regge exchange. We find this more appealing.

ACKNOWLEDGMENTS

We thank Gabriele Veneziano for informative discussions on his results.

We wish to express our appreciation to Mrs. Connie Gentzler for assistance in preparing the manuscript.

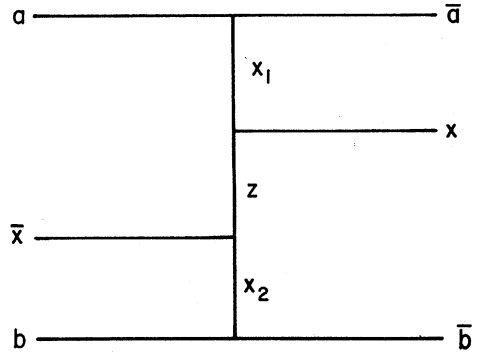

FIG. 8. Tree diagram used for calculating the asymptotic limit in the central region.

APPENDIX A: CALCULATION OF LIMITING DISTRIBUTIONS

We give here the details of the calculation of the appropriate asymptotic behaviors and discontinuities of the dual six-point functions necessary to obtain the limiting distributions (1.3)–(1.6). Our method is first to calculate the appropriate asymptotic behavior [see Eqs. (2.1)–(2.6)] and then to take the discontinuity in M^2; i.e., we take the discontinuity of the Regge asymptotic form of the amplitude.

(i) Fragmentation Region. We calculate the contribution of the diagram $\left[\begin{smallmatrix} a & \bar{a} \\ \bar{x} & x \\ b & \bar{b} \end{smallmatrix}\right]$ in the fragmentation region for b (the contribution of the other three diagrams can be obtained by permuting b and $\bar{x}$ and/or $\bar{b}$ and x [see Eq. (2.8)]). For this diagram the standard dual six-point function is

$$\left[\begin{smallmatrix} a & \bar{a} \\ \bar{x} & x \\ b & \bar{b} \end{smallmatrix}\right] = \int_0^1\int_0^1\int_0^1 dx_1dx_2dy\, x_1^{-\alpha_{b\bar{x}}-1}(1-x_1)^{-\alpha_{a\bar{x}}-1}x_2^{-\alpha_{\bar{b}x}-1}(1-x_2)^{-\alpha_{\bar{a}x}-1}y^{-\alpha-1}(1-y)^{-\alpha_{a\bar{a}}-1}$$
$$\times(1-x_1y)^{-\alpha_{a\bar{a}\bar{x}}+\alpha_{a\bar{x}}+\alpha_{a\bar{a}}}(1-x_2y)^{-\alpha_{a\bar{a}x}+\alpha_{\bar{a}x}+\alpha_{a\bar{a}}}(1-x_1x_2y)^{-\alpha_{a\bar{a}}-\alpha_{b\bar{b}}+\alpha_{a\bar{a}\bar{x}}+\alpha_{a\bar{a}x}}. \tag{A1}$$

We take the asymptotic limit α, α_{ab}, $\alpha_{\bar{a}\bar{b}}$, $\alpha_{a\bar{x}}$, $\alpha_{\bar{a}x} \to -\infty$, where the integral representation (A1) is defined and then continue to the desired region α, α_{ab}, $\alpha_{\bar{a}\bar{b}} \to +\infty$ and $\alpha_{a\bar{x}}$, $\alpha_{\bar{a}x} \to -\infty$ [see Eqs. (2.1) and (2.2′)]. In this limit we observe that the dominant contribution to the integral comes from $y \approx 1$. Using the usual techniques, i.e., substituting $y = 1 + z/\alpha$ and taking the leading-order term, we can do one integration to obtain

$$\left[\begin{smallmatrix} a & \bar{a} \\ \bar{x} & x \\ b & \bar{b} \end{smallmatrix}\right] \underset{\text{frag } b}{\sim} \Gamma(-\alpha_{a\bar{a}})\int_0^\infty\int_0^\infty dz_1dz_2z_1^{-\alpha_{b\bar{x}}-1}(1+z_1)^{\alpha_{b\bar{x}}+\alpha_{b\bar{b}}-\alpha_{a\bar{a}x}}z_2^{-\alpha_{\bar{b}x}-1}(1+z_2)^{\alpha_{\bar{b}x}+\alpha_{b\bar{b}}-\alpha_{a\bar{a}\bar{x}}}$$
$$\times(1+z_1+z_2)^{-\alpha_{a\bar{a}}-\alpha_{b\bar{b}}+\alpha_{a\bar{a}\bar{x}}+\alpha_{a\bar{a}x}}(-\alpha-\alpha_{a\bar{x}}z_1-\alpha_{\bar{a}x}z_2)^{\alpha_{a\bar{a}}}, \tag{A2}$$

where we have made the change of variables $z_1 = x_1/(1-x_1)$, $z_2 = x_2/(1-x_2)$. We immediately observe that in the limit we have taken, the right-hand side (A2) is purely real. As we continue α, α_{ab}, and $\alpha_{\bar{a}\bar{b}}$ to their respective physical regions (2.1), an imaginary part develops due to the last factor in the integrand. Care must be taken when we take the discontinuity in α so as not to enclose singularities in α_{ab} and $\alpha_{\bar{a}\bar{b}}$ (see discussion of Sec. II A). Of course, the diagram we are considering has no singularities in these variables, but the other three diagrams do. A detailed study shows that for all four diagrams the discontinuity in $\alpha(M^2)$ is given by

$$\text{Disc}_{M^2}\left[\begin{smallmatrix} a & \bar{a} \\ \bar{x} & x \\ b & \bar{b} \end{smallmatrix}\right] \underset{\text{frag } b}{\sim} \frac{\pi}{\Gamma(\alpha_{a\bar{a}}+1)}\alpha^{\alpha_{a\bar{a}}}\left(-\frac{\alpha_{a\bar{x}}}{\alpha}\right)^{\alpha_{b\bar{x}}}\left(-\frac{\alpha_{\bar{a}x}}{\alpha}\right)^{\alpha_{\bar{b}x}}$$
$$\times\int_0^\infty\int_0^\infty dy_1dy_2\,\theta(1-y_1-y_2)\,y_1^{-\alpha_{b\bar{x}}-1}y_2^{-\alpha_{\bar{b}x}-1}\left(1-\frac{\alpha}{\alpha_{a\bar{x}}}y_1\right)^{\alpha_{b\bar{x}}+\alpha_{b\bar{b}}-\alpha_{a\bar{a}x}}\left(1-\frac{\alpha}{\alpha_{\bar{a}x}}y_2\right)^{\alpha_{\bar{b}x}+\alpha_{b\bar{b}}-\alpha_{a\bar{a}\bar{x}}}$$
$$\times\left(1-\frac{\alpha}{\alpha_{a\bar{x}}}y_1-\frac{\alpha}{\alpha_{\bar{a}x}}y_2\right)^{-\alpha_{a\bar{a}}-\alpha_{b\bar{b}}+\alpha_{a\bar{a}\bar{x}}+\alpha_{a\bar{a}x}}(1-y_1-y_2)^{\alpha_{a\bar{a}}}, \tag{A3}$$

with the appropriate permutation of b and $\bar{x}$ and/or $\bar{b}$ and x. In writing (A3) we have made the further change of variables $y_1 = -(\alpha_{a\bar{x}}/\alpha)z_1$, $y_2 = -(\alpha_{\bar{a}x}/\alpha)z_2$. We remark that the integrand of (A3) is purely real and any imaginary part comes from the factors $(-\alpha_{ab}/\alpha)^{\alpha_{b\bar{x}}}$ and $(-\alpha_{\bar{a}\bar{b}}/\alpha)^{\alpha_{\bar{b}x}}$ appearing for the other three diagrams. Although individual diagrams may be complex, the functions $f_b{}^x$ and $h_b{}^x$ are purely real as required since the sum[16] of four diagrams is taken.

(ii) Central Region. There are two ways of calculating the asymptotic behavior in the central region. We can obtain it by taking the $\alpha_{b\bar{x}}$, $\alpha_{\bar{b}x} \to -\infty$ limit of the results above for the fragmentation region for b (or the $\alpha_{a\bar{x}}$, $\alpha_{\bar{a}x} \to -\infty$ limit for the fragmentation region for a). Alternatively, we can take the limit (2.4) directly on the six-point function. These two ways give the same result. Here we use the second method as it leads directly to an elegant expression.

It is convenient to begin with the choice of variables corresponding to the tree diagram shown in Fig. 8:

$$\left[\begin{smallmatrix} a & \bar{a} \\ \bar{x} & x \\ b & \bar{b} \end{smallmatrix}\right] = \int_0^1\int_0^1\int_0^1 dx_1dzdx_2x_1^{-\alpha_{a\bar{a}}-1}z^{-\alpha_{a\bar{a}x}-1}x_2^{-\alpha_{b\bar{b}}-1}(1-x_1)^{-\alpha_{a\bar{x}}-1}(1-z)^{-\alpha_{a\bar{a}\bar{x}}-1}(1-x_2)^{-\alpha_{b\bar{x}}-1}$$
$$\times(1-x_1z-x_2z+x_1x_2z)^{\alpha_{a\bar{a}x}}\left[\frac{(1-x_1z-x_2z+x_1x_2z)}{(1-x_1z)(1-x_2z)}\right]^{\alpha-\alpha_{a\bar{x}}-\alpha_{b\bar{x}}}, \tag{A4}$$

where we have taken $\alpha_{a\bar{x}} = \alpha_{\bar{a}x}$, $\alpha_{b\bar{x}} = \alpha_{\bar{b}x}$.

The asymptotic behavior is first obtained in the limit α, $\alpha_{a\bar{x}}$, $\alpha_{b\bar{x}} \to -\infty$. The important region of integration is $x_1, x_2 \approx 0$. The usual exponentiation procedure easily gives

$$\begin{bmatrix} a & \bar{a} \\ \bar{x} & x \\ b & \bar{b} \end{bmatrix}_{\text{central}} (-\alpha_{a\bar{x}})^{\alpha_{a\bar{a}}} (-\alpha_{b\bar{x}})^{\alpha_{b\bar{b}}} \int_0^1 dz\, z^{-\alpha_{a\bar{a}x}-1} (1-z)^{-\alpha_{a\bar{a}\bar{x}}-1} \mathcal{V}\left(\alpha_{a\bar{a}}, \alpha_{b\bar{b}}; \frac{\bar{\kappa}}{z(1-z)}\right), \tag{A5}$$

where

$$\bar{\kappa} \equiv \alpha_{a\bar{x}} \alpha_{b\bar{x}} / \alpha < 0 \tag{A6}$$

and

$$\mathcal{V}(\alpha_1, \alpha_2; x) = \int_0^\infty \int_0^\infty dy_1 dy_2 y_1^{-\alpha_1 - 1} y_2^{-\alpha_2 - 1} \exp\left(-y_1 - y_2 + \frac{y_1 y_2}{x}\right) \tag{A7}$$

is the usual two-Reggeon–single-particle vertex function.[17] Considered as a real analytic function of x, $\mathcal{V}$ has a branch cut for $0 \leq x < \infty$. This branch cut through (A6) gives a cut in α for $0 \leq \alpha < \infty$. Therefore, we have

$$\text{Disc}_{M^2} \begin{bmatrix} a & \bar{a} \\ \bar{x} & x \\ b & \bar{b} \end{bmatrix}_{\text{central}} (-\alpha_{a\bar{x}})^{\alpha_{a\bar{a}}} (-\alpha_{b\bar{x}})^{\alpha_{b\bar{b}}} \int_0^1 dz\, z^{-\alpha_{a\bar{a}x}-1} (1-z)^{-\alpha_{a\bar{a}\bar{x}}-1} \left[\text{Disc}_x \mathcal{V}\left(\alpha_{a\bar{a}}, \alpha_{b\bar{b}}; x = \frac{\kappa}{z(1-z)}\right)\right], \tag{A8}$$

where we have now replaced $\bar{\kappa}$ by κ since they are asymptotically equal. Further, from (A7), we easily obtain

$$\begin{aligned} \text{Disc}_x \mathcal{V}(\alpha_1, \alpha_2; x) &\underset{x \geq 0}{=} \frac{\pi}{\Gamma(\alpha_2 + 1)} \int_x^\infty dy_1 y_1^{-\alpha_1 - 1} (y_1/x - 1)^{\alpha_2} e^{-y_1} \\ &= \pi e^{-x} x^{-\alpha_1} \Psi(\alpha_2 + 1, -\alpha_1 + \alpha_2 + 1; x), \end{aligned}$$

which can be written in a symmetric form:

$$\text{Disc}_x \mathcal{V}(\alpha_1, \alpha_2; x) \underset{x \geq 0}{=} \pi e^{-x} \left[\frac{\Gamma(\alpha_1 - \alpha_2)}{\Gamma(\alpha_1 + 1)} x^{-\alpha_1} \Phi(\alpha_2 + 1, -\alpha_1 + \alpha_2 + 1; x) + \frac{\Gamma(\alpha_2 - \alpha_1)}{\Gamma(\alpha_2 + 1)} x^{-\alpha_2} \Phi(\alpha_1 + 1, -\alpha_2 + \alpha_1 + 1; x)\right], \tag{A9}$$

where Ψ and Φ are the usual confluent hypergeometric functions.[31]

To obtain the asymptotic behavior for large $\kappa = p_\perp^2 + m_x^2$, we make use of the asymptotic behavior of Ψ, which yields[32]

$$\text{Disc}_x \mathcal{V}(\alpha_1, \alpha_2; x) \underset{x \to +\infty}{\sim} \pi x^{-\alpha_1 - \alpha_2 - 1} e^{-x}, \tag{A10}$$

and of the fact that $z \approx \frac{1}{2}$ dominates (A8). This yields Eq. (3.9). We note that in the fragmentation region for b, large $p_\perp$ corresponds to large $\alpha_{b\bar{x}} = \alpha_{\bar{b}x}$. For large $\alpha_{b\bar{x}}$, Eq. (A3) has a dominant behavior coming from $y_1, y_2 \approx \frac{1}{2}$, which is easily seen to give a factor

$$\left[1 - \frac{2\alpha_{a\bar{x}}}{\alpha}\right]^{2\alpha_{b\bar{x}}} \approx \left[-\left(1 - \frac{2\alpha_{ab}}{\alpha}\right)\right]^{2\alpha_{b\bar{x}}}. \tag{A11}$$

This factor provides a cutoff in transverse momentum in the fragmentation region and goes smoothly over to the behavior $e^{-4\kappa}$ in the central region.

We have already argued in Sec. II that only the diagram computed above contributes in the central region. However, it is interesting to use Plahte's relations[10] to examine more closely the behavior of the other diagrams. We find, for example,

$$\text{Disc}_{M^2} \begin{bmatrix} a & \bar{a} \\ b & \bar{b} \\ \bar{x} & x \end{bmatrix} = \frac{\sin\pi(\alpha_{ab} + \alpha_{b\bar{x}} - \alpha_{a\bar{x}}) \sin\pi(\alpha_{\bar{a}\bar{b}} + \alpha_{\bar{b}x} - \alpha_{\bar{a}\bar{x}})}{\sin\pi(\alpha_{ab} - \alpha_{a\bar{x}}) \sin\pi(\alpha_{\bar{a}\bar{b}} - \alpha_{\bar{a}\bar{b}x})} \text{Disc}_{M^2} \begin{bmatrix} a & \bar{a} \\ \bar{x} & x \\ b & \bar{b} \end{bmatrix},$$

where, on the right-hand side,

$$\alpha_{b\bar{b}} \to \alpha_{a\bar{a}} + \alpha_{x\bar{x}} - \alpha_{x\bar{x}\bar{b}} - \alpha_{x\bar{x}b} - 1,$$
$$\alpha_{a\bar{x}} \to -\alpha_{ab} - \alpha_{b\bar{x}} + \alpha_{ab\bar{x}} - 1,$$
$$\alpha_{\bar{a}x} \to -\alpha_{\bar{a}\bar{b}} - \alpha_{\bar{b}x} + \alpha_{\bar{a}\bar{b}x} - 1, \tag{A12}$$
$$\alpha_{a\bar{a}x} \to -\alpha_{\bar{b}x} + \alpha_{b\bar{x}} + \alpha_{a\bar{a}} - \alpha_{x\bar{x}b} - 1,$$
$$\alpha_{a\bar{a}\bar{x}} \to -\alpha_{b\bar{x}} + \alpha_{\bar{b}x} + \alpha_{a\bar{a}} - \alpha_{x\bar{x}\bar{b}} - 1,$$

and

$$\mathrm{Disc}_{M^2}\begin{bmatrix} a & \bar{a} \\ b & x \\ \bar{x} & \bar{b} \end{bmatrix} = \frac{\sin\pi(\alpha_{ab} + \alpha_{b\bar{x}} - \alpha_{ab\bar{x}})}{\sin\pi(\alpha_{ab} - \alpha_{ab\bar{x}})}\,\mathrm{Disc}_{M^2}\begin{bmatrix} a & \bar{a} \\ \bar{x} & x \\ b & \bar{b} \end{bmatrix},$$

where, on the right-hand side,

$$\alpha_{b\bar{b}} \to -\alpha_{\bar{x}\bar{b}} - \alpha_{b\bar{x}} + \alpha_{b\bar{b}\bar{x}} - 1,$$
$$\alpha_{a\bar{x}} \to -\alpha_{ab} - \alpha_{b\bar{x}} + \alpha_{ab\bar{x}} - 1, \tag{A13}$$
$$\alpha_{a\bar{a}\bar{x}} \to -\alpha_{b\bar{x}} + \alpha_{\bar{b}x} + \alpha_{a\bar{a}} - \alpha_{x\bar{x}\bar{b}} - 1.$$

Suppose we apply the replacements (A12) and (A13) to (A8) to obtain the behavior of these diagrams in the central region.[33] Owing to the replacements of $\alpha_{b\bar{b}}$, except in special cases like $\alpha(0) = -m^2 = 1$, these diagrams will have a different dependence on the asymptotic variable $\alpha_{b\bar{x}}$.[34] Regardless of the sine factors, only the diagram $\left[\begin{smallmatrix} \bar{a} & x \\ a & \bar{x} \\ b & \bar{b} \end{smallmatrix}\right]$ can have, in general, the behavior $(-\alpha_{b\bar{x}})^{\alpha_{b\bar{b}}} = (-\alpha_{b\bar{x}})^{\alpha_V}$, which is required to give a finite, nonzero limiting distribution.

APPENDIX B: BEHAVIOR OF RESONANCES IN MISSING MASS

We calculate the contribution of a given resonance in M^2 in the six-point dual amplitude and show that for large mass it agrees with the limiting distributions of Sec. III and Appendix A, thus confirming the duality of the resonance and Regge behaviors discussed in Sec. IV.

In order to simplify the computations, we consider only an illustrative example with the following particular choice for the nonasymptotic trajectory functions:

$$\alpha_{a\bar{a}} = \alpha_{b\bar{b}} = \alpha_{x\bar{x}} = \alpha_{a\bar{a}x} = \alpha_{a\bar{a}\bar{x}} = \alpha_{a\bar{a}\bar{b}} = \alpha_{b\bar{b}a} = \alpha_{b\bar{b}\bar{a}} = -1. \tag{B1}$$

In this case, Eq. (3.1) becomes

$$\begin{bmatrix} a & \bar{a} \\ \bar{x} & x \\ b & \bar{b} \end{bmatrix} = \int_0^1\int_0^1\int_0^1 dx_1 dx_2 dy\, x_1^{-\alpha_{b\bar{x}}-1}(1-x_1)^{-\alpha_{a\bar{x}}-1}x_2^{-\alpha_{\bar{b}x}-1}(1-x_2)^{-\alpha_{\bar{a}x}-1}y^{-\alpha-1}(1-x_1y)^{\alpha_{a\bar{x}}}(1-x_2y)^{\alpha_{\bar{a}x}},$$

from which one easily obtains

$$\mathrm{Res}_{\alpha=N}\begin{bmatrix} a & \bar{a} \\ \bar{x} & x \\ b & \bar{b} \end{bmatrix} = \pi\sum_{l=0}^{N}\frac{\Gamma(-\alpha_{a\bar{x}}+N-l)\Gamma(-\alpha_{b\bar{x}}+N-l)}{\Gamma(N-l+1)\Gamma(-\alpha_{a\bar{x}}-\alpha_{b\bar{x}}+N-l)}\,\frac{\Gamma(-\alpha_{\bar{a}x}+l)\Gamma(-\alpha_{\bar{b}x}+l)}{\Gamma(l+1)\Gamma(-\alpha_{\bar{a}x}-\alpha_{\bar{b}x}+l)}. \tag{B2}$$

Inspecting (B2) for large N, one can see that the main contribution comes for both N and $N-l$ large. Therefore, we take $l = zN$, $(N-l) = (1-z)N$ and make the replacement

$$\sum_{l=0}^{N} \to N\int_0^1 dz.$$

Then, using Stirling's formula, we obtain

$$\mathrm{Res}_{\alpha=N}\begin{bmatrix} a & \bar{a} \\ \bar{x} & x \\ b & \bar{b} \end{bmatrix} \underset{\text{large } N}{\sim} \frac{\pi}{N}\int_0^1 \frac{dz}{z(1-z)}\left(1-\frac{\alpha_{a\bar{x}}}{zN}\right)^{\alpha_{b\bar{x}}}\left(1-\frac{\alpha_{b\bar{x}}}{zN}\right)^{\alpha_{a\bar{x}}} e^{\kappa/z}\left(1-\frac{\alpha_{\bar{a}x}}{(1-z)N}\right)^{\alpha_{\bar{b}x}}\left(1-\frac{\alpha_{\bar{b}x}}{(1-z)N}\right)^{\alpha_{\bar{a}x}} e^{\kappa/(1-z)}. \tag{B3}$$

For the fragmentation of b we must take the further limit $\alpha_{a\bar{x}}, \alpha_{\bar{a}x} \to -\infty$ in (B3). We then have

$$\mathrm{Res}_{\alpha=N}\begin{bmatrix} a & \bar{a} \\ \bar{x} & x \\ b & \bar{b} \end{bmatrix} \underset{\text{frag } b}{\underset{\text{large } N}{\sim}} \frac{\pi}{N}\int_0^1 \frac{dz}{z(1-z)}\left(1-\frac{\alpha_{a\bar{x}}}{zN}\right)^{\alpha_{b\bar{x}}}\left(1-\frac{\alpha_{\bar{a}x}}{(1-z)N}\right)^{\alpha_{\bar{b}x}}. \tag{B4}$$

One can show that (B4) is equivalent to (A3) for the special choice of trajectories (B1).

In the central region we must take $\alpha_{a\bar{x}}, \alpha_{b\bar{x}}, \alpha_{\bar{a}x}, \alpha_{\bar{b}x} \to -\infty$ with fixed κ. It is easy to see that

$$\mathrm{Res}_{\alpha=N}\begin{bmatrix} a & \bar{a} \\ \bar{x} & x \\ b & \bar{b} \end{bmatrix} \underset{\text{central}}{\overset{\text{large } N}{\sim}} \frac{\pi}{N}\int_0^1 \frac{dz}{z(1-z)} e^{-\kappa/z(1-z)}, \tag{B5}$$

which agrees with (A8) for the choice (B1).

The dual expression (B2) for the discontinuity in M^2 is also useful for studying many other features of limiting distributions, for example, the symmetry properties (2.7).

---

*Work supported in part through funds provided by the U. S. Atomic Energy Commission under Contract Nos. AT(30-1)-2098 and NYO-2262TA-237.

[1]For a review see D. Sivers and J. Yellin, Rev. Mod. Phys. 43, 125 (1971).

[2]See, for example, E. L. Berger and G. C. Fox, Phys. Rev. 188, 2120 (1969).

[3]A. H. Mueller, Phys. Rev. D 2, 2963 (1970).

[4]J. Benecke, T. T. Chou, C. N. Yang, and E. Yen, Phys. Rev. 188, 2159 (1969).

[5]C. E. DeTar, C. E. Jones, F. E. Low, J. H. Weis, J. E. Young, and C.-I Tan, Phys. Rev. Letters 26, 675 (1971).

[6]Thus we focus our attention on the individual narrow-resonance contributions, although a more general approach involving finite-energy sum rules in the missing mass could be applied.

[7]This is analogous to the conjecture of Bloom and Gilman for inelastic electron scattering. [E. D. Bloom and F. J. Gilman, Phys. Rev. Letters 25, 1140 (1970).] There is, however, an important difference (see Sec. IV).

[8]For further discussion see C.-I Tan, Phys. Rev. D 3, 788 (1971).

[9]K. Bardakci and H. Ruegg, Phys. Rev. 181, 1884 (1969); Chan Hong-Mo and Tsou Sheung-Tsun, Phys. Letters 28B, 485 (1969); C. J. Goebel and B. Sakita, Phys. Rev. Letters 22, 257 (1969); Z. Koba and H. B. Nielsen, Nucl. Phys. B10, 633 (1969).

[10]E. Plahte, Nuovo Cimento 66A, 713 (1970). We wish to thank Andrew Hanson for informative discussions on the subject matter of this reference.

[11]In general, the intercepts of some of the trajectories on the right side of Eq. (2.7) are shifted. The explicit results are given in Eqs. (A12) and (A13). In the case $m^2 = -\alpha(0) = -1$, no intercepts are shifted and we have relationships between the unmodified B_6 functions.

[12]For fixed momentum transfer, see G. Veneziano, Nuovo Cimento 57A, 196 (1968).

[13]The rate at which the sine factors vanish along a ray depends upon the angle of the ray. We regard the necessity for introducing a phase angle and this consequence as unpleasant but unavoidable features of the model, which are closely related to the presence of poles in the physical region.

[14]As usual the units are chosen such that the trajectory slope $b=1$.

[15]A remark is in order here to eliminate a possible source of confusion. Since $(p_a+p_{\bar{a}}+p_x)^2=(p_a+p_{\bar{a}}+p_{\bar{x}})^2 = m_x^2$, if x lies on the leading trajectory in the $a\bar{a}x$ and $a\bar{a}\bar{x}$ channels, as would normally be the case, then $\alpha_{a\bar{a}x} = \alpha_{a\bar{a}\bar{x}} = 0$. Although the original expression (3.1) is not defined in this case, the expressions for the limiting distributions are defined since they are discontinuities in an overlapping variable and thus have no poles at $\alpha_{a\bar{a}x} = \alpha_{a\bar{a}\bar{x}} = 0$. This is clearly seen, for example, in (3.7); the exponential vanishing of $\mathrm{Disc}_x v$ as its argument goes to infinity assures the convergence of the integral.

[16]We can allow for the inclusion of internal symmetry factors by introducing signatures τ.

[17]K. Bardakci and H. Ruegg, Phys. Letters 28B, 342 (1968).

[18]See for example E. W. Anderson *et al.*, Phys. Rev. Letters 16, 855 (1966); J. L. Day *et al.*, *ibid.* 23, 1055 (1969); Dennis B. Smith *et al.*, *ibid.* 23, 1064 (1969).

[19]D. G. Crabb *et al.*, Phys. Rev. Letters 21, 830 (1968).

[20]We illustrate this by an explicit example in Appendix B.

[21]For large M^2, but for $s \gg M^2$, Eq. (4.4) implies an explicit M^2 dependence for the logarithmic width of the forward peak. If $d\sigma/dt = s^{2\alpha(t)}e^{ct}$ then $c = c_0 - 2b\ln M^2$, where b is the trajectory slope. The peak widens weakly with increasing M^2 at fixed s.

[22]This is where we differ with the Bloom-Gilman analysis of the threshold behavior of electroproduction structure functions. They were able to assume that the resonances trace out the scaling curve even for small N; we are not able to do so.

[23]This could correspond to keeping the scattering angle $z \sim 1 + 2\alpha_{a\bar{x}}/\alpha_{ab} \sim -1 - 2\alpha_{b\bar{x}}/\alpha_{ab}$ real.

[24]One may wish to give $-\alpha_{a\bar{x}}$ and $-\alpha_{b\bar{x}}$ smaller phases in magnitude than α_{ab} in order to keep $\kappa = (-\alpha_{a\bar{x}})(-\alpha_{bx})/\alpha_{ab}$ real in this case.

[25]There is, in any case, not much freedom since a "wrong" choice of nonzero phase would lead to obviously unphysical exponentially growing phase-dependent factors.

[26]The nine terms in (4.5) correspond to the nine diagrams of Fig. 3. Only 7 of the terms give any contribution to the distributions, since with the conventional phase choices in the Regge and fixed-angle regions, it is easily seen that two of the terms

$$\frac{\sin\pi(\alpha_{ab}+\alpha_{a\bar{x}})\sin\pi(\alpha_{\bar{a}\bar{b}}+\alpha_{\bar{b}x})}{\sin\pi\alpha_{ab}\sin\pi\alpha_{\bar{a}\bar{b}}}$$

and

$$\frac{\sin\pi(\alpha_{ab}+\alpha_{b\bar{x}})\sin\pi(\alpha_{\bar{a}\bar{b}}+\alpha_{\bar{a}x})}{\sin\pi\alpha_{ab}\sin\pi\alpha_{\bar{a}\bar{b}}}$$

do not contribute in any region.

[27]A. DiGiacomo, S. Fubini, L. Sertorio, and G. Veneziano, Phys. Letters 33B, 171 (1970).

[28]Kenneth G. Wilson, Acta Phys. Austriaca 17, 38 (1964); C. E. DeTar, Phys. Rev. D 3, 128 (1971).

[29]D. Gordon and G. Veneziano, Phys. Rev. D 3, 2116 (1971).

lished).

[30]M. A. Virasoro, Phys. Rev. D 3, 2834 (1971).

[31]Bateman Manuscript Project, *Higher Transcendental Functions*, edited by A. Erdélyi (McGraw-Hill, New York, 1953), Vol. 1, pp. 255 and 257.

[32]This behavior implies an analogous exponential vanishing of the imaginary part of the five-point function. It would be very interesting to have a physical explanation for this behavior.

[33]The same results are obtained by a direct calculation of the asymptotic behaviors.

[34]Explicitly,

$$\alpha_{a\bar{a}}+\alpha_{x\bar{x}}-\alpha_{x\bar{x}\bar{b}}-\alpha_{x\bar{x}b}-1$$
$$=\alpha_{b\bar{b}}+[-a_{\bar{b}\bar{b}}+a_{a\bar{a}}+a_{x\bar{x}}-\alpha_{x\bar{x}\bar{b}}(m_b^2)-\alpha_{x\bar{x}b}(m_b^2)-1],$$
$$-\alpha_{\bar{x}\bar{b}}-\alpha_{b\bar{x}}+\alpha_{b\bar{b}\bar{x}}-1$$
$$=\alpha_{b\bar{b}}+[-a_{bb}-a_{\bar{x}b}-a_{b\bar{x}}-2m_x^2-2m_b^2+\alpha_{b\bar{b}\bar{x}}(m_x^2)-1].$$

For reasonable masses and intercepts both brackets are negative so that the diagram in (A8) has a higher power. However, for example, for sufficiently negative intercepts the second bracket is positive.

PHYSICAL REVIEW D VOLUME 4, NUMBER 2 15 JULY 1971

Failure of the Eikonal Approximation for the Vertex Function in a Boson Field Theory*

E. Eichten† and R. Jackiw‡
Laboratory for Nuclear Science and Physics Department, Massachusetts Institute of Technology, Cambridge, Massachusetts 02139
(Received 16 February 1971)

By an explicit calculation of the high-energy behavior of the three-point function in the $\lambda\phi^3$ theory, through terms of order λ^5, we demonstrate that the eikonal approximation for generalized ladder exchange fails in that model, for this vertex function. In a given order, it underestimates the exact asymptote.

The high-energy behavior of Feynman graphs and of field-theoretic amplitudes is currently studied with the help of the eikonal approximation.[1,2] This technique has been extended from its original domain of applicability, fermion–vector-boson models, to other field theories, in particular the $\lambda\phi^3$ model.[3] The latter model has two important features which make it an attractive theoretical laboratory: (1) The (hopefully) inessential complications of spin are absent and the Feynman rules are correspondingly simple; (2) Regge-type behavior has been established in this theory. Unfortunately, there is no proof that the amplitudes of this model, when evaluated in the eikonal approximation, bear any relation to the high-energy asymptote of the *exact* expressions, even in perturbation theory. Indeed, a recent investigation by Tiktopoulos and Treiman[4] of certain scattering graphs, involving crossed ladder exchanges, indicates that there may exist groups of Feynman diagrams whose high-energy behavior is not necessarily given by the eikonal approximation.

The purpose of this paper is to publicize the fact that the generalized ladder exchange graphs, contributing to the three-point function (vertex function) in the $\lambda\phi^3$ theory, when calculated to fifth-order perturbation theory, possess "leading logarithms" in the high-energy region which are not properly given by the eikonal approximation. This result makes use of an old calculation, performed some years ago by one of us (R.J.) in connection with the evaluation of the high-energy behavior of the vertex function in a spinor–vector-meson theory: quantum electrodynamics.[5] For the latter theory, the eikonal approximation correctly describes the high-energy asymptote, at least order by order in perturbation theory.[6]

The use of the eikonal techniques to calculate the vertex function is just as plausible as the analogous computation of the scattering amplitude since the eikonal approximation is correct in this context for spinor–vector-meson theories.[6] Because our calculation is in a (relatively) low order of perturbation theory, all the contributing ladder exchange graphs can be analyzed completely, and it is evi-

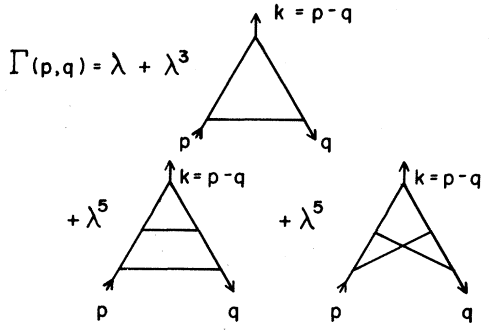

FIG. 1. Generalized ladder graphs, through λ^5, which contribute to $\Gamma(p,q)$.